Gonbad Kavous University

Journal of New Approaches in Water Engineering and Environment

Online ISSN: 2981-0280

Homepage: https://nawee.gonbad.ac.ir

Experimental and Numerical Investigation of Riprap Stability for Protection Downstream of the Spillway

Mehdi Sayahi [1], Ali Reza Masjedi [2*]✉, Amin Bordbar [3], Mohammad Heidarnejad [4], Aslan Egdernezhad [5]

[1] Department of Water Science Engineering, Faculty of Agriculture and natural sciences, Ahv.C., Islamic Azad University, Ahvaz, Iran.
[2] Department of Water Science Engineering, faculty of Agriculture and natural sciences, Ahv.C., Islamic Azad University, Ahvaz, Iran.
[3]Department of Water Science Engineering, faculty of Agriculture and natural sciences, Ahv.C., Islamic Azad University, Ahvaz, Iran.
[4] Department of Water Science Engineering, faculty of Agriculture and natural sciences, Ahv.C., Islamic Azad University, Ahvaz, Iran.
[5] Department of Water Science Engineering, faculty of Agriculture and natural sciences, Ahv.C., Islamic Azad University, Ahvaz, Iran.

Article Info

Article type:
Research Article

Article history:
Received 03 February 2025
Revised 26 June 2025
Accepted 20 July 2025
Published online 28 Agust 2025

Keywords:
Flip bucket spillway
Tail water
Riprap
Flow 3D

ABSTRACT

Objective: This research was conducted to investigate the stability of the riprap downstream of the flip bucket spillway. For this purpose, a flip bucket spillway model with four angles and four sill lengths was used. In clear water, riprap with four different diameters was used in experiments to measure flow depth.

Material and Methods: In all experiments, the flow strength was adjusted, and the water depth upstream of the spillway was measured immediately downstream after the flow passed through the spillway. The exit jet from the triangular launcher was then formed, followed by the formation of a hydraulic jump. In each step, the necessary variables were measured. The Froude Number in the unstable condition of the riprap, the relative diameter of the riprap in the unstable condition, and the stability number of the riprap were calculated.

Results and Discussion: This research showed that the most stability number, related to the spillway with a sill angle of 45 degrees and a relative length of 0.17, and the least stability number was observed in a spillway with a sill angle of 15 degrees and a relative length of 0.05. To this end, 8 experiments performed on the physical model were simulated in FLOW-3D, and the results were compared.

Conclusions: In the study of the physical model, an increase in the threshold length improved the energy dissipation performance of the structure. However, in the mathematical model, this increase deteriorated the performance at angles of 15° and 25° but enhanced the performance at angles of 35° and 45°. In the mathematical model, the flow projected from buckets at 35° and 45° caused a hydraulic jump further from the structure.

*Corresponding author, Email: Al.masjedi@iau.ac.ir

Cite this article: Sayahi, M., Masjedi, A.R., Bordbar, A., Heidarnejad, M., Egdernezhad, A. (2025). Experimental and ıumerical Investigation of Riprap Stability for Protection Downstream of the Spillway, j*ournal of New Approaches in Water Engineering and Environment*, 4(2), 20-37. https://doi.org/ 10.22034/nawee.2025.504263.1134

Publisher: Gonbad Kavous University.
DOI: https://doi.org/10.22034/nawee.2025.504263.1134

1.Introduction

Energy consumption in spillways is necessary to protect the structure and prevent erosion downstream of the structure. Spillways of flip buckets are structures used for energy consumption, and their use is developing daily. Considering that the flow in spillways is supercritical, as a result, the kinetic energy of the flow at the end of the spillway is very high and can cause erosion downstream of the spillway. Therefore, a spillway needs an energy-consuming structure at the end part to reduce the excess output energy, minimize erosion, and check the spillway downstream. Downstream scouring of hydraulic structures is one of the major issues that has always attracted the attention of engineers and designers. The scour hole created downstream of hydraulic structures causes the flow under the structure to increase, resulting in the scour hole moving towards the structure. This can threaten the dam's stability, spillway, and related structures, and even lead to their failure. Numerous approaches have been proposed to prevent and reduce scouring in hydraulic structures, which can be classified into two direct and indirect methods. The substrate's resistance increases against the applied stresses in the direct method. This work is done by strengthening the existing materials with more resistant materials; one of the usual and economical methods is to use concrete blocks and ripraps. Modifying the flow pattern around the desired structure in the indirect method reduces the destructive force and erosion. In recent years, spillway flip buckets have received more attention due to the economic benefits of this structure compared to other amortizes, such as the relaxation pond.

Posey (1974) considered the movement of the first aggregates of the aggregate as a criterion for failure. Parola (1993) used a three-layer aggregate with a colored middle layer. He considered the failure threshold of the aggregate to be when the colored layer was visible after 30 minutes without movement. Chiew (1995), in his research, considered a 15-minute period for observing the failure of the aggregate around the bridge piers, and related the instability of the aggregate layer to the condition of its complete failure. In fact, in his opinion, the movement of a few aggregates from the aggregate layer is not enough to cause its failure.

Lauchlan and Melville (2001) considered the performance of the aggregate layer to be acceptable before the depth of the scour hole in it reached 20%, the maximum depth of subsidence, without the presence of aggregate. Another variable in the design of a gravel separator is the thickness and characteristics of the filter layer. The tendency of fine particles in the pores of the gravel separator bed to escape leads to its screen-like destruction. The solution to prevent this type of destruction is to increase the thickness of the gravel separator layer and place a filter layer between the fines and the gravel separator. Worman (1989) showed in his experiments that if the thickness of the gravel separator layer is sufficient, there will be no need to place a filter layer underneath. Verman concluded that the performance of a multilayer riprap system with different grain sizes would be the same as that of a single homogeneous layer with a smaller layer thickness. Masjedi et al. (2017) conducted a study to investigate the effect of roughness on the stability of riprap around a cylindrical bridge abutment. Experiments were conducted in a laboratory flume using two types of riprap relative densities with four different diameters at a constant flow rate in clear water. The results of this study showed that the stability of riprap around a cylindrical abutment depends on two factors: The Froude number at the failure threshold and the relative diameter of the riprap. Also, under the same conditions, the presence of roughness in the cylindrical abutment in the arch increases the stability of the riprap around the cylindrical abutment.

Yoon et al. (1995) proposed a more accurate and comprehensive method for designing riprap around the base by modifying and developing the Parola method. In this method, the effect of various parameters on riprap stability is applied as correction factors to the stability number.

Salmati and Masoudian (2025), studied Analysis of Hydraulic Performance of Hinged Sluice Gate in Spillway and Gate Modes, the study employs experimental and numerical methods to evaluate flow characteristics and gate performance. The findings indicate that the hinged sluice gate significantly influences flow stability and energy dissipation, with optimal performance observed in spillway mode under specific flow conditions, providing insights for improving gate design in spillway systems.

Ebrahimi et al. (2024), studied Effect of Opening Dimensions on Scour Around Permeable Groynes. the results demonstrate that larger openings reduce scour depth around groynes by allowing better flow passage, offering practical implications for designing protective structures to mitigate erosion downstream of hydraulic structures like spillways.

Cheng et al. (2024) studied TDG generation in a ski-jump spillway with a full or partial-flip bucket. The results indicate that the use of the partial-flip bucket at the end of the spillway significantly disperses the water flow and yields better energy dissipation effects. At low flow rates (lower than 400 m3/s for the dam in this study), there is little difference in the downstream TDG saturation between the traditional fully-flip bucket and the partial-flip bucket; the average difference is 1.6 % in three cases with a low flow rate. However, at high flow rates (higher than 400 m3/s), the partial-flip bucket generates more TDG compared to the traditional fully-flip bucket, reaching up to 6.2 % at the maximum flow rate. This phenomenon stems from significant changes in the hydrodynamics of the stilling basin at high flow rates due to variations in the flip bucket type. When strict control of TDG generation is necessary downstream of dams, the use of the partial-flip bucket should be carefully considered. This is because, at high flow rates, the partial-flip bucket might result in higher TDG saturation than the fully-flip bucket.

Dah-Mardeh et al. (2024) studied a Laboratory investigation to control downstream scour in a specific model of stepped spillway by six-legged concrete elements (A-Jack). The results of the protected bed (PB) experiments with SLC elements illustrated their significant effect in scour reduction. In the case of PB, the maximum depth and length of the relative scour hole decreased by about 59%–100% and 29%–100%, respectively. Several experimental equations of regression analysis were expanded to evaluate the relative scour components. Moreover, the analysis of scour borderlines equations was investigated with the presence of SLC armor. The study results proposed an innovative scour control for foundation protection by SLC armoring counteractions (Dah-Mardeh, Azizyan, Bejestan, Parsaie, & Rajaei, 2024).

Mirzaee et al. (2023) studied applying soft computing techniques to estimate the scouring depth formed by crossing jets. The prediction results showed that the Multi-Layer Perceptron (MLP) model performs best among the other models tested here. The Pearson correlation coefficient, root mean square error, and normalized root mean square error for the MLP model were 0.9527, 0.9039, and 19.36% for the test phase, respectively. Furthermore, based on the sensitivity analysis, the parameters, for instance, tailwater depth and vertical jet angle, have the highest and lowest effects for predicting the scouring depth of a plunge pool, respectively.

Fuladipanah et al. (2023) studied the precise forecasting of scour depth downstream of a flip bucket spillway through data-driven models. In this study, DDMs are developed to predict the

scouring depth downstream of the flip-bucket spillway. The study's novelty lies in the use of field data and the Froude number parameter as an input variable. The innovation presented in this research can be summarized in two significant aspects: (i) utilization of field-measured data: the research incorporates the novel approach of utilizing field-measured data, which adds a valuable real-world dimension to the study; (ii) simplification of DDMs: the research simplifies the complexity associated with DDMs by relying on a single readily input variable, namely the Froude number. This streamlines the modeling process and enhances its practical applicability. In the current paper, an exploration of the capabilities and potential of the SVM, the GEP, the MLP, and the MARS has been undertaken. The objective is to predict the scour depth downstream of a flip-bucket spillway utilizing field-collected data. In addition to these DDMs, five empirical equations have also been employed. The findings of this investigation are as follows (Fuladipanah, Azamathulla, Tota-Maharaj, Mandala, & Chadee, 2023).

All four DDMs exhibit acceptable potential for predicting scour depth. Nevertheless, the MARS model outperforms the other models in terms of all evaluation indicators, indicating superior performance.

However, in the direct comparison between the DDM and the regression model, the results unequivocally establish that the MARS model possesses a substantial and statistically significant advantage over the empirical equation.

Achour et al. (2022), Studied on control of the hydraulic jump by a thin-crested sill in a rectangular channel new experimental considerations In their research, the regulation of the hydraulic jump by a thin-crested sill is determined by three dimensionless parameters: the incident Froude number F1, the relative position X/h2 of the sill, and the relative height of the sill S = s/h1. The 1950 tests involved only three values of the relative position of the threshold, that is X/h 2= 3; 5 and 10. This resulted in a diagram of three curves showing the variation in the relative sill height S as a function of the incident Froude number F 1. If the point defined by the coordinates (S; F 1) is located between two curves of the diagram, then it is necessary to carry out a binding interpolation.

Rashki Ghaleh Nou et al. (2020), Management of bed erosion downstream of a ski-jump spillway was achieved through the use of a combination of six-legged concrete structures and appropriately sized riprap. The experiments were conducted on five distinct drainage channels with Froude numbers between 3.42 and 15, comparing an unprotected layer (baseline test) with a protected layer featuring six-legged concrete elements of fixed dimensions and average diameters of 9 mm and 20 mm (Rashki Ghaleh Non, Azhdary Moghaddam, Shafaei Bajestan, & Azamathulla, 2020). layers with two sizes of riprap. .51 and three underwater depths. The results of the baseline tests showed that the maximum scour depth increased with increasing flow rate at different seabed depths. Moreover, the maximum scour depth increases for each condition as the stability value increases. From the tests on the protective floor, it was concluded that using six-legged concrete elements caused jets to penetrate through the pores between the protective cover and the scour, ultimately leading to the collapse of the protective layer. Additionally, this combination reduced the amount of material used to protect the bed from 56.6% to 100%. Several empirical relationships were developed using experimental data to predict the maximum scour depth of different protection alternatives under various conditions. A blueprint for determining the required riprap size was also proposed by defining bed scour as a criterion for the stability of six-legged concrete.

Eskandari et al. (2020) experimentally investigated the effects of different shapes and configurations of the gap on the downstream blade flashing dimensions. When the results were compared with the empirical formula, a high correlation was observed between them. By comparison, the Talaimović equation gave more accurate results in controlled experiments, and the Damle-A and Damle-B equations gave more accurate results in experiments with rectangular and triangular slotted blades in the maze (Eskandari, Heidarnejad, Masjedi, Purmohammadi, & Kamanbedast, 2020).

Previous research shows that although many studies have been conducted on triangular spillways, fewer studies have been undertaken on applying numerical methods in triangular spillway analysis. Therefore, triangular spillway analysis is conducted using the Flow3D numerical model in this research.

2.Material and Methods

2.1. Dimensional Analysis

Using riprap downstream of a spillway strengthens the streambed and increases its resistance to flow-induced shear stresses. One of the most important parameters for checking the resistance of riprap to flow-induced shear stress is the dimensionless parameter stability number. The effective parameters in this experiment, assuming that the fluid properties are constant, are such that the following relationship exists between the parameters affecting the stability of the riprap and the energy consumption in the equilibrium state:

$$f1(B,\alpha,L,d_{50},y_t,V_t,g,G_s) \qquad (1)$$

In Eq. (1), B is the width of the spillway, α is the angle of the sill, L is the length of the sill, d_{50} is the average diameter of the riprap, y_t is the depth of the flow instability, V_t is the speed of the flow in unstable conditions, g is the acceleration of gravity, G_s is the density of the riprap. Using Buckingham's theory, Eq. (1) becomes dimensionless as follows:

$$f_2\left(\frac{d_{50}}{y_t},\alpha,\frac{L}{B},Fr_t,SN_t\right) \qquad (2)$$

In Eq. (2), d_{50}/y_t is the relative diameter of the riprap, α is the angle of the sill, L/B is the relative length of the sill, Fr_t is the Froude number in unstable conditions, and SN_t is the stability number.

2.2.Experimental Modeling

The experiments in this study were performed hydraulically in a laboratory trough measuring 8 meters long, 0.5 meters wide, and 0.6 meters high in Ahvaz Branch, Islamic Azad University. The channel walls were made of transparent glass, allowing the flow state to be seen. The bottom of the channel was considered smooth, stable, and without slope. The overflow folding bucket model was manufactured according to USBR standards with a height of 40 cm and a length of 53.4 cm. In this research, sixteen models of spillway flip buckets with four angles of sill (2.5, 4.5, 6.5, and 8.5 cm $L/B = 0.05,0.09,0.13,0.17$) and four angles of sill (15, 25, 35, and 45 degrees) were made of fiberglass (Figure 1).

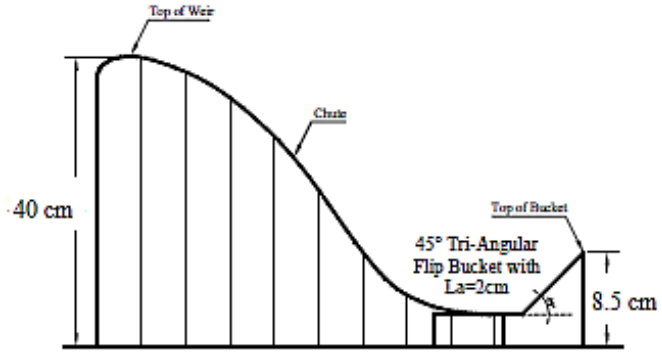

Figure 1- Sketch of a flip bucket spillway

The ripraps used in this study were made from round natural materials with a constant density of 2.1 and an average diameter of 9.52, 11.23, 12.7, and 23.1 mm. To determine the gravel area downstream of the spillway, an equilibrium test was performed without placing gravel downstream to check the scour hole's maximum dimensions. In this test, each spillway was run individually without a dam in a layer of sand approximately 15 cm thick at a maximum flow rate of 25 l/s during a 4-hour long-term test. At the end of the test, the pump was stopped, and the end valve was closed to drain the water in the channel slowly, so as not to affect the formation's topography. Once the water had been completely drained from inside the irrigation canal, the extent of the scour downstream of the overflow section was measured to the nearest millimeter using a laser depth gauge. At the end of the experiment, after emptying the irrigation canal, the area of the scour pit for experimentation was selected as a rectangle with a length of 50 cm and a width of 40 cm downstream of the overflow. Based on the work of Melville et al. (2007) the shape of the checkered stone arrangement downstream of the spillway was assumed to be rectangular and flush with the river bed material. Moreover, according to the criteria of Melville et al., the thickness of the tile layer was selected to correspond to twice the average diameter of the tiles. To conduct the tests, first, the spillway flip bucket model was installed in a place 7 meters away from the beginning of the direct flume to provide the necessary length to create a uniform flow upstream. Then, the riprap with a thickness twice the average diameter of the riprap and aligned with the bed material was placed downstream of the spillway. The test was carried out in such a way that first, the pump was used, the flow entered the flume, and the flow rate was then regulated using special valves and measured at a triangular weir with sharp edges at the front of the channel. The volumetric method was used to calibrate the triangular edge weir. The spill depth was measured at a distance of 60 cm upstream of the spillway for each spill. This was because it was far from the upstream water level profile changes. After setting the desired flow rate, gradually close the end valve until the water depth is below the overflow or the water depth is deeper. The depth of the underwater increased until a high hydraulic jump was formed after the jet hit the bottom of the rock (Karimaei Tabarestani, 2020). The purpose of this jump is to measure the depth of the unsteady flow after passing through the projectile (Karimaei Tabarestani, 2021). Then the end valve was slowly opened to create the flow conditions for a small movement of the ballast particles. After ensuring that the depth of the flow along the flume was constant, the movement of the gravel particles was visually checked. When the particles of the riprap began to move slowly, this condition was referred to as the movement threshold. At this point, the flow depth was measured at a fixed point within the channel and considered the unsteady flow depth. In all experiments, the initial depth of the hydraulic jump could not be directly measured due to the presence of air in the flow at the downstream edge of the projectile. To measure this depth, the flow after the projectile was supercritical with the formation of a high-distance hydraulic jump from the projectile, and the

secondary depth of the hydraulic jump was measured, assuming constant momentum on both sides of the hydraulic jump. The primary depth of the hydraulic jump was then obtained from the relationship of the conjugate depths of the hydraulic jump, regardless of friction losses. Following this, the energy on both sides of the spillway was calculated using depth and speed measurements from the Bernoulli Equation. Energy losses in different projectiles were then calculated (Figure 2).

Figure 2-Spillway of a flip bucket and riprap at the downstream

2.3.Numerical Modeling

The FLOW-3D program is a simulation tool with a wide range of applications suitable for analyzing complex liquid flow issues, including temporal three-dimensional free-surface flows with intricate geometry. This computer program employs the finite volume method with a rectangular structured mesh (Marusi et al., 2014). The discretized conditions used are similar in form to discretized finite difference conditions. The present study used the RNG model to close the Reynolds time-averaged equations.

FLOW-3D was used to perform the numerical simulation, and the governing transient equations were solved using the finite volume method. This program utilized the fractional area-volume obstacle representation (FAVOR) algorithm to define the geometry within the finite volume method (Fadaei-Kermani and Barani, 2014). This algorithm considers obstacles in the flow field as fractional values between 0 and 1 within computational cells. Specifically, the fractional volume or area will equal 1 if the obstacle fills the entire cell. The free surface is determined by the volume-of-fluid (VOF) method. The velocity and pressure terms are coupled in continuity and energy equations using previous pressure and velocity values.

This program solves the resulting semi-implicit equations iteratively using relaxation methods. The modeling work used the GMRES method as the implicit pressure solver. The numerical model in FLOW-3D creates a three-dimensional structured mesh consisting of rectangular cuboid cells for the flow field under study. For this purpose, a three-dimensional model was created in the AutoCAD program based on the specifications of the laboratory model. Then, the model was imported into the FLOW-3D computer program to generate the mesh or use the VOF and FAVOR tools to define the boundaries and the computational mesh.

After inputting the geometry data into the program and specifying the boundaries of the primary and secondary channels in the domain, the mesh was generated using the VOF and FAVOR methods. The optimal mesh dimensions were selected according to the desired accuracy and the time allocated for the computations. Furthermore, the mesh was adjusted so that the mesh lines were perpendicular.

In this investigation, some parts of the spillway from which information was collected were assigned a finer mesh, while other parts were assigned a coarser mesh. Based on the measurements of the physical model, the length and width of the channel at a distance of 7

meters from the straight flume were determined to be 50 cm and 40 cm, respectively, in the numerical model, and the mesh was generated accordingly. On average, the number of elements in the models was 1,583,606, 1,579,054, and 82,090 in the X, Y, and Z directions. After setting up boundary conditions and initial conditions, the water flow was simulated.
The Sketch Mesh Setup for the Spillway is shown in Figure 3. Table 1 displays grid information for the mesh block.

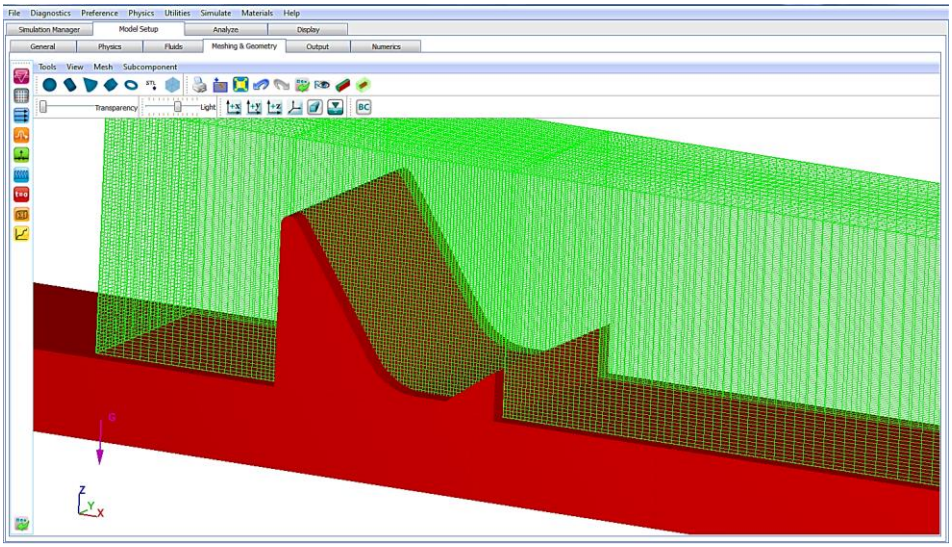

Figure 3- Sketch Mesh Setup for Spillway

Table 1- grid information for mesh block

No.	Subject	Block	Total Number of Real Cells	Minimum Cell Size	Maximum Cell Size	Maximum Adjacent Cell Size Ratio
1	X	1	180	0.0083428	0.0391717	1.06437
	Y	1	30	0.0166667	0.0166667	1
	Z	1	70	0.0086956	0.02	2.3

2.4. Turbulence Models and Boundary Conditions

In this research, the mesh field was set to be uniform and fairly fine to obtain results that are as close as possible to the experimental results and reduce computation time. It should be noted that the average simulation time for each flow rate was 24 hours, but this was reduced to about 8 hours using the available powerful system. The RNG turbulence model was used to solve the Navier-Stokes equations. The boundary conditions were defined as follows: Pressure for the upper boundary condition, Wall for the lower boundary condition, Volume Flow Rate for the inlet boundary condition, and Outflow for the outlet boundary condition. The Wall option was also selected for the left and right flow boundaries.

2.5. Boundary Conditions:

The boundary conditions for the problem were specified in the Boundaries section:

- The inlet boundary was set to Volume Flow Rate, with the specified Gulf Stream rate.
- The outlet boundary was set to Fixed Level.

- The left and right boundaries were set to Divider, which is used to separate fluid and solid media. The normal and tangential velocities on the divider boundary are both considered zero in this condition.
- The Symmetry option was chosen for the upper boundary.

Figure 4 shows the boundary conditions for the spillway.

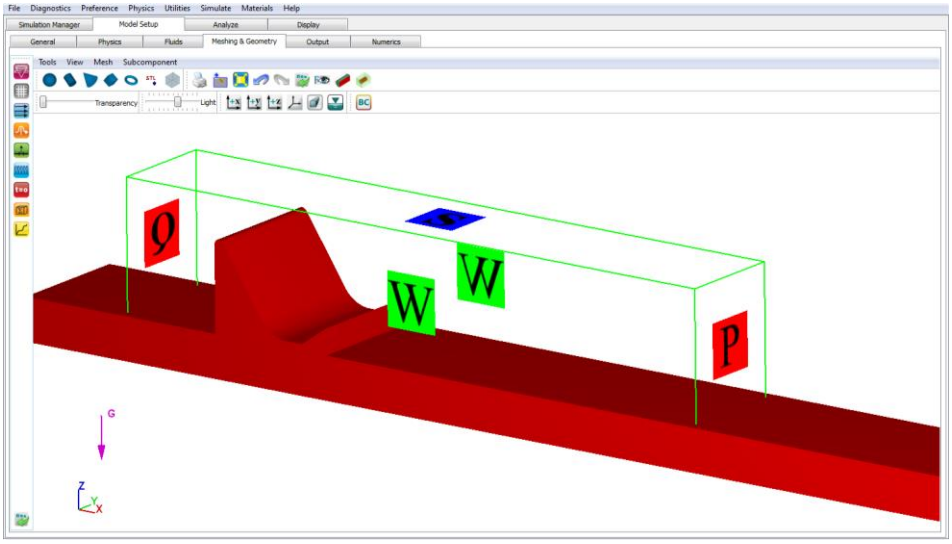

Figure 4- Boundary Conditions for spillway

2.6.Calibration

Given the nature of the design, both the roughness coefficient and the turbulence model can be used to achieve more accurate physical and simulation results. Therefore, the experimental results were initially compared to physical models for various roughness and turbulence cases. A comparison of the turbulence models showed that the RNG turbulence model produced the closest results. Additionally, changes in roughness had a minimal impact on the results.

3.Results and Discussion

3.1.Experimental Modeling

In all experiments, the flow strength was adjusted, and the water depth upstream of the spillway was measured immediately downstream after the flow passed through the spillway. The exit jet from the triangular launcher was then formed, followed by the formation of a hydraulic jump. In each step, the necessary variables were measured. The Froude Number in the unstable condition of the riprap, the relative diameter of the riprap in the unstable condition, and the stability number of the riprap were calculated. Table 2 presents the results of the experiments.

Table 2- Characteristic of riprap at the downstream of the spillway

L/B	α (deg.)	d_{50} (mm)	$y_t(cm)$	V_t (m)	Fr_t	d_{50}/y_t	SN_t
0.05	15	9.52	14.3	0.35	0.29	0.07	1.09
0.09	15	9.52	14	0.36	0.30	0.068	1.11
0.13	15	9.52	13.7	0.37	0.31	0.069	1.14
0.17	15	9.52	13.2	0.38	0.33	0.072	1.18
0.05	25	9.52	12.9	0.39	0.34	0.074	1.21
0.09	25	9.52	12.5	0.40	0.36	0.076	1.25
0.13	25	9.52	12.1	0.41	0.38	0.079	1.30
0.17	25	9.52	11.8	0.42	0.39	0.080	1.32
0.05	35	9.52	11.5	0.43	0.41	0.083	1.36
0.09	35	9.52	11.1	0.45	0.43	0.086	1.40
0.13	35	9.52	10.8	0.46	0.45	0.088	1.44

L/B	α (deg.)	d_{50} (mm)	$y_t(cm)$	V_t (m)	Fr_t	d_{50}/y_t	SN_t
0.17	35	9.52	10.2	0.49	0.49	0.218	1.53
0.05	45	9.52	9.6	0.52	0.54	0.099	1.62
0.09	45	9.52	9.2	0.54	0.57	0.0103	1.69
0.13	45	9.52	8	0.63	0.71	0.119	1.95
0.17	45	9.52	7.6	0.66	0.76	0.125	2.05
0.05	15	11.23	13.9	0.36	0.3	0.081	1.03
0.09	15	11.23	13.5	0.37	0.32	0.083	1.06
0.13	15	11.23	13	0.38	0.34	0.086	1.10
0.17	15	11.23	12.7	0.39	0.35	0.088	1.13
0.05	25	11.23	12.2	0.41	0.37	0.092	1.18
0.09	25	11.23	11.8	0.42	0.39	0.095	1.22
0.13	25	11.23	11.4	0.44	0.41	0.098	1.26
0.17	25	11.23	10.9	0.46	0.44	0.103	1.32
0.05	35	11.23	10.7	0.47	0.46	0.105	1.34
0.09	35	11.23	10.4	0.48	0.48	0.108	1.38
0.13	35	11.23	10.1	0.49	0.50	0.111	1.42
0.17	35	11.23	9.4	0.53	0.55	0.119	1.53
0.05	45	11.23	9.1	0.55	0.58	0.123	1.58
0.09	45	11.23	8.4	0.60	0.66	0.134	1.71
0.13	45	11.23	7.8	0.64	0.73	0.144	1.84
0.17	45	11.23	7.1	0.7	0.84	0.158	2.02
0.05	15	12.7	13.5	0.37	0.32	0.094	1.00
0.09	15	12.7	13.1	0.38	0.34	0.097	1.03
0.13	15	12.7	12.6	0.40	0.36	0.101	1.07
0.17	15	12.7	12	0.42	0.38	0.106	1.126
0.05	25	12.7	11.6	0.43	0.40	0.109	1.164
0.09	25	12.7	11.1	0.45	0.43	0.114	1.217
0.13	25	12.7	10/8	0.46	0.45	0.117	1.251
0.17	25	12.7	10.3	0.48	0.483	0.123	1.311
0.05	35	12.7	9.8	0.51	0.52	0.129	1.378
0.09	35	12.7	9.5	0.53	0.54	0.134	1.421
0.13	35	12.7	9.1	0.55	0.58	0.139	1.484
0.17	35	12.7	8.8	0.57	0.61	0.144	1.534
0.05	45	12.7	8.2	0.61	0.68	0.155	1.647
0.09	45	12.7	7.8	0.64	0.73	0.163	1.732
0.13	45	12.7	7.2	0.69	0.83	0.176	1.876
0.17	45	12.7	6.8	0.73	0.90	0.187	1.986
0.05	15	23.1	13	0.38	0.34	0.178	0.77
0.09	15	23.1	12.7	0.39	0.35	0.182	0.788
0.13	15	23.1	12.1	0.41	0.38	0.191	0.828
0.17	15	23.1	11.7	0.43	0.40	0.197	0.856
0.05	25	23.1	11.1	0.45	0.43	0.208	0.902
0.09	25	23.1	10.7	0.47	0.46	0.216	0.936
0.13	25	23.1	10.4	0.48	0.47	0.222	0.963
0.17	25	23.1	9.8	0.51	0.52	0.236	1.02
0.05	35	23.1	9.4	0.53	0.55	0.246	1.065
0.09	35	23.1	9.0	0.56	0.59	0.26	1.112
0.13	35	23.1	8.7	0.57	0.62	0.27	1.151
0.17	35	23.1	8.3	0.60	0.67	0.28	1.207
0.05	45	23.1	7.7	0.65	0.75	0.30	1.300
0.09	45	23.1	7.3	0.68	0/80	0.316	1.371
0.13	45	23.1	6.9	0.72	0/88	0.33	1.451
0.17	45	23.1	6.3	0.79	1.101	0.37	1.589

3.2.Effect of Threshold Angle on Riprap Stability

Figure 5 shows the stability of the check riprap downstream of the spillway flip bucket based on the Froude number of instability. The study considered four sill angles of 15, 25, 35, and 45 degrees, four relative sill lengths of 0.05, 0.09, 0.13, and 0.17, and four diameters of the riprap: 9.52, 11.23, 12.7, and 23.1 mm.

The results on the graph indicate that the Froude number of instability at the threshold of movement plays a significant role in the stability of sill formations. With a constant density, the stability number at the threshold of movement decreases at different angles of the sill as the Froude number of instability increases. A higher Froude number in the depth of instability leads to increased flow speed, resulting in decreased stability of the ripraps across all average diameters at all sill angles.

Furthermore, the study found that the spillway exhibited the highest stability number with a sill angle of 45 degrees. In comparison, the lowest stability number was observed with a sill angle of 15 degrees. Increasing the sill angle in the spillway causes more flow to be directed upwards, leading to higher energy consumption in the spillway. This results in the downstream flow requiring less energy and the riprap being more stable under these conditions.

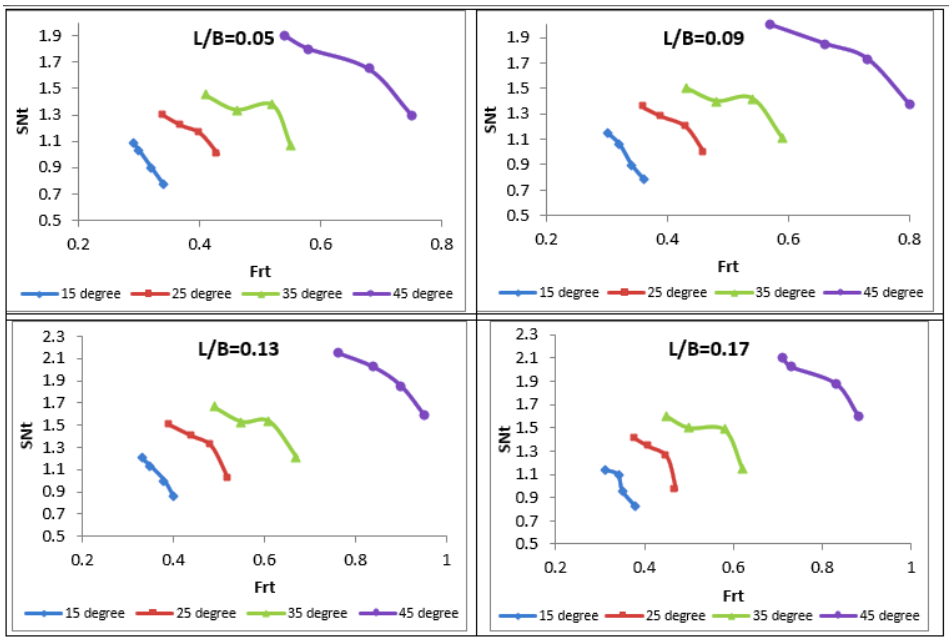

Figure 5- Stability of riprap based on the Froude Number of instability at different angles of the sill

3.3.Effect of Threshold Angle on Riprap Stability

Figure 6 shows the stability of the riprap downstream of the flip bucket spillway based on the Froude number of instability. It includes four sill angles of 15, 25, 35, and 45 degrees, four relative lengths of the sill (0.05, 0.09, 0.13, and 0.17), and four diameters of the riprap (9.52, 11.23, 12.7, and 23.1 mm).

The graphs indicate that as the Froude number increases, the flow speed also increases, leading to decreased stability of the riprap for all average stone diameters and lengths. The highest stability number was observed with a relative length of 0.17, while the lowest stability number was seen with a length of 0.05.

Increasing the length of the sill extends the flow path on the spillway, resulting in higher energy consumption. This causes the flow to transfer downstream with less energy, leading to more stable riprap formations under these conditions.

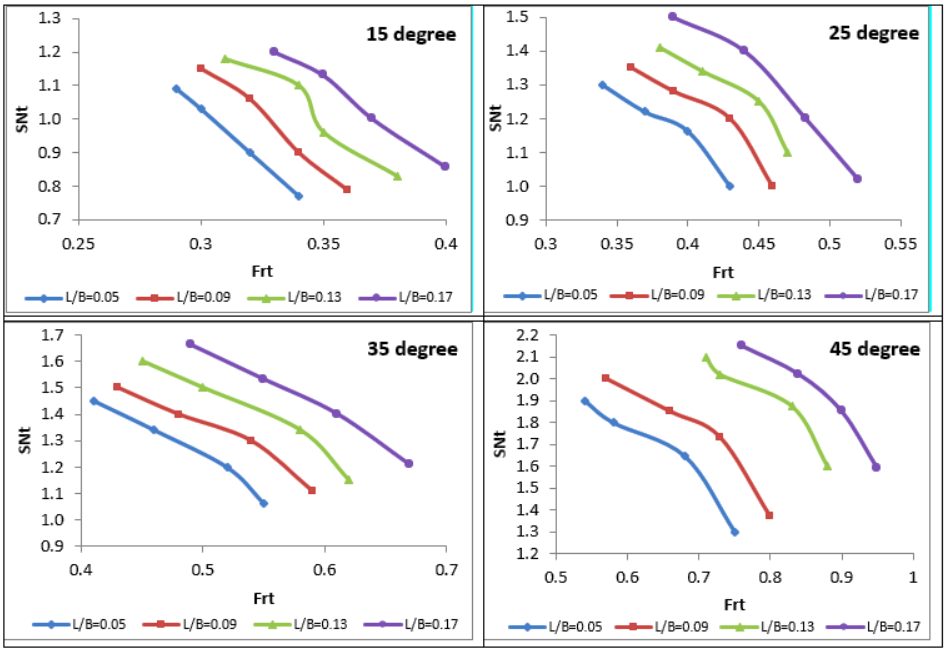

Figure 6- Stability of riprap based on the Froude Number of instability for different lengths of the sill

3.4.The stability of the riprap is based on the relative diameter of the riprap

Figures 7 and 8 display the stability of riprap based on its relative width at four sill angles of 15, 25, 35, and 45 degrees, and four riprap widths of 9.52, 11.23, 12.7, and 23.1 mm. The charts indicate that the relative width of the riprap is also an important factor in determining its stability. The stability index at the critical point decreases with an increase in the relative width of the riprap. Essentially, as the size of the riprap increases, its effectiveness in providing stability decreases.

Moreover, Figure 7 shows that the stability index for a weir with a 45-degree sill angle is significantly higher than that of a 15-degree sill angle. Additionally, Figure 8 reveals that the highest stability is achieved at a relative sill length of 0.17, while the lowest stability is observed at 0.05. These findings highlight the impact of riprap width on stability and are consistent with previous studies by other researchers.

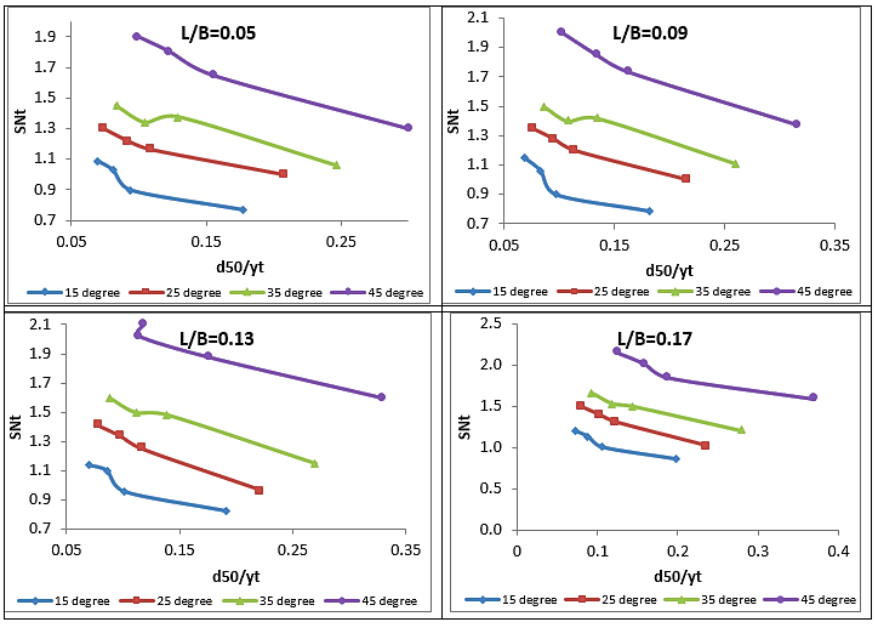

Figure 7- The stability of the riprap is based on the relative diameter of the riprap in different sill angles

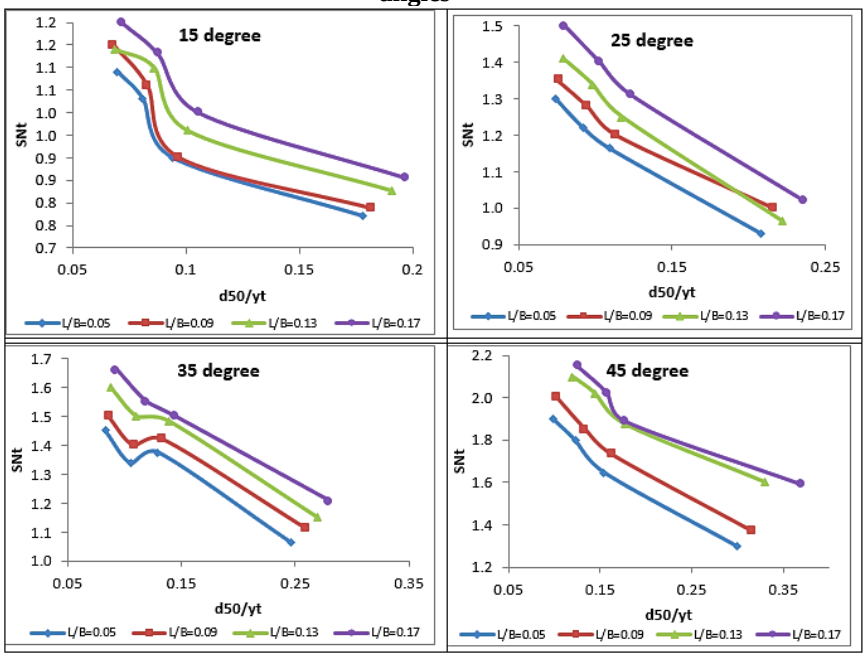

Figure 8- The stability of the riprap is based on the relative diameter of the riprap in different sill lengths

3.5.Numerical Modeling

After the tests were conducted and the results were collected, the standard spillway condition was used to analyze the flow rate through curved labyrinth spillways. The measurement data were used to determine the flow rate and the total hydraulic head for the spillways inside the channel. The following section presents the model outputs. These outputs will also be compared to the results of the physical model. A three-dimensional view of the model output is shown in Figure 9.

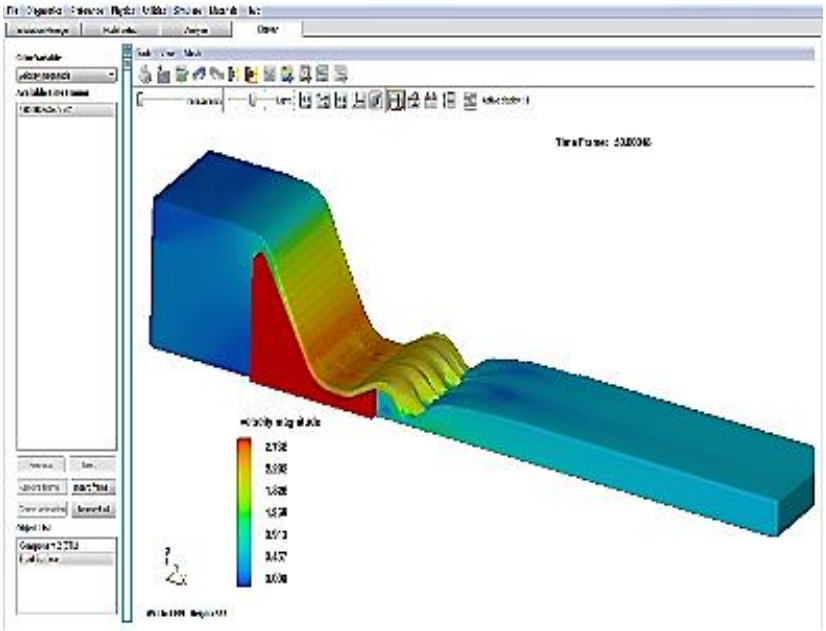

Figure 9- Three-dimensional view of the model output

The longitudinal section shows the flow velocity over the spillway in the results of the numerical model for various threshold lengths and angles (Figure 10a to 10h).

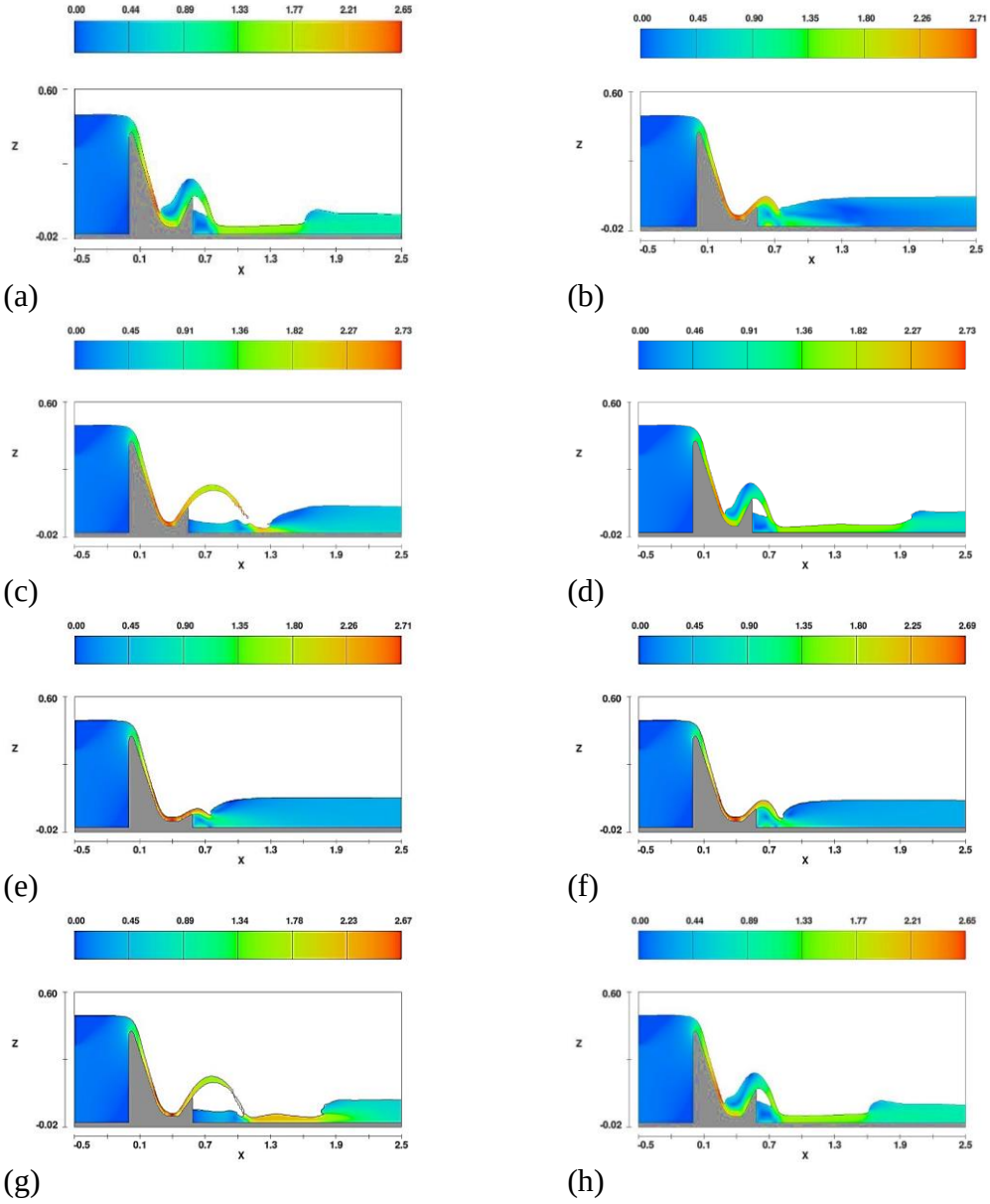

Figure 10- The longitudinal section of the flow velocity over the spillway in the Numerical model with a different threshold length and an angle; (a) threshold length of 4.5 cm and an angle of 15°, (b) threshold length of 4.5 cm and an angle of 25°, (c) threshold length of 4.5 cm and an angle of 35°, (d) threshold length of 4.5 cm and an angle of 45°, (e) threshold length of 8.5 cm and an angle of 15°, (f) threshold length of 8.5 cm and an angle of 25°, (g) threshold length of 8.5 cm and an angle of 35°, (h) threshold length of 8.5 cm and an angle of 45°

3.6. Comparison of Numerical and Experimental Model Results

A comparison was made between the numerical and experimental results. The most noteworthy vitality scattering within the tested models happened within the triangular bucket at a point of 45°. The finest spillway models regarding stream rate and release coefficient with known

geometric parameters (spillway tallness) were chosen for a more precise comparison and reenacted. In this way, 34 three-dimensional reenactments were carried out. After the spillway geometries were built and imported into the FLOW-3D program, they were fit, and their boundary and gulf conditions were indicated. For this reason, 16 physical tests and 8 numerical reenactments were performed, Tables 3 and 4, and Figure 11.

Table 3- Physical model result

No	Threshold length (cm)	Threshold angle (deg)	Depth after hydraulic jump (m)	Flow velocity after the jump (m/s)	Landing number after jump	Water depth before jump (m)	Flow velocity before jump (m/s)	Specific energy before the jump (m)	ΔE (m)	$(\Delta E/E_0)*100$ (%)
1	4/5	15	0/14	0/3472	0/2922	0/0214	2/3357	0/2996	0/2104	41/26
2	8/5	15	0/14	0/3650	0/3149	0/0232	2/1525	0/2595	0/2505	49/12
3	4/5	25	0/13	0/3788	0/3329	0/0247	2/0278	0/2343	0/2757	54/06
4	8/5	25	0/13	0/3968	0/3570	0/0265	1/8846	0/2076	0/3024	59/29
5	4/5	35	0/12	0/4237	0/3939	0/0293	1/7048	0/1775	0/3325	65/19
6	8/5	35	0/11	0/4673	0/4562	0/0338	1/4777	0/1452	0/3648	71/53
7	4/5	45	0/1	0/5263	0/5453	0/0398	1/2559	0/1202	0/3898	76/42
8	8/5	45	0/08	0/6173	0/6926	0/0486	1/0292	0/1026	0/4074	79/88

Table 4- FLOW3D Model result

No	Threshold length (cm)	Threshold angle (deg)	Depth after hydraulic jump (mm)	Water depth before jump (m)	Flow velocity before jump (m/s)	Specific energy before the jump (m)	y0 (m)	v0 (m/s)	E0 (m)	ΔE (m)	$(\Delta E/E_0)*100$ (%)
1	4/5	15	0/14	0/0340	1/4706	0/1443	0/4926	0/1400	0/4936	0/3493	70/77
2	8/5	15	0/14	0/0330	1/5152	0/1501	0/4926	0/1400	0/4936	0/3435	69/60
3	4/5	25	0/13	0/0300	1/6667	0/1716	0/4926	0/1400	0/4936	0/3220	65/23
4	8/5	25	0/13	0/0290	1/7241	0/1806	0/4926	0/1400	0/4936	0/3130	63/42
5	4/5	35	0/12	0/0320	1/5625	0/1565	0/4926	0/1400	0/4936	0/3371	68/30
6	8/5	35	0/11	0/0350	1/4286	0/1391	0/4926	0/1400	0/4936	0/3545	71/83
7	4/5	45	0/1	0/0370	1/3514	0/1301	0/4926	0/1400	0/4936	0/3635	73/64
8	8/5	45	0/08	0/0390	1/2821	0/1228	0/4926	0/1400	0/4936	0/3708	75/12

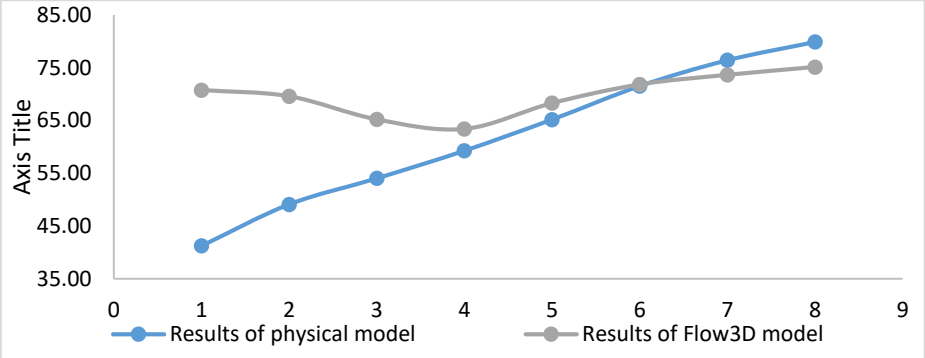

Figure 11- Comparison of the results of the Flow3D model and the physical model

4.Conclusion

This research investigated the influence of threshold length and triangular bucket angle on the performance of an ogee spillway. To this end, 8 of the experiments performed on the physical model were simulated in FLOW-3D, and the results were compared.

1. In the study of the physical model, an increase in the threshold length improved the energy dissipation performance of the structure. However, in the mathematical model, this increase deteriorated the performance at angles of 15° and 25° but enhanced the performance at angles of 35° and 45°.
2. In the physical model, an increase in the projection angle improved the energy dissipation performance of the structure. In contrast, this performance first deteriorated and then improved in the mathematical model. Because, in the mathematical model, a projection angle of 15° caused a larger submerged jump, leading to higher energy dissipation.
3. In the mathematical model, the flow projected from buckets at angles of 35° and 45° caused a hydraulic jump further from the structure. This led to a reduction in the structure's energy dissipation performance. This phenomenon was not observed in the physical model.

Author Contributions

Data Availability Statement

Acknowledgements

The authors deeply appreciate the Khuzestan Water and Power Authority for providing the test facilities.

Ethical Considerations

Funding

No funding was received from any financial organization to conduct this research.

Conflict of Interest

The authors declare that they have no known financial or non-financial competing interests in any material discussed in this paper.

References

Achour, B., Amara, L., Mehta, D. 2022. Control of the hydraulic jump by a thin-crested sill in a rectangular channel: New experimental considerations. *LARHYSS Journal*, (50):31-48.

Chiew, Y.M. 1995. Mechanics of riprap failure. *Journal of Hydraulic Engineering*, 121(9): 635-643. DOI: 10.1061/(ASCE)0733-9429(1995)121:9(635)

Dah-Mardeh, A., Azizyan, G., Bejestan, M.S., Parsaie, A., Rajaei, S.H. 2024. Laboratory investigation to control of downstream scour in a specific model of stepped spillway by six-legged concrete elements (A-Jack). *Ocean Engineering*, 304:117815. DOI: 10.1016/j.oceaneng.2024.117815

Ebrahimi, Z., Ramezani, Y., Dastourani, M. 2024. Effect of opening dimensions on scour around permeable groynes, New Approaches in Water and Environmental Engineering, 85–105. doi: 10.22034/nawee.2024.489481.1118

Eskandari, A., Heidarnejad, M., Masjedi, A., Purmohammadi, M.H., Kamanbedast, A. 2020. Experimental investigation on the effect of different slot shapes and configurations on scour dimension downstream of flip buckets. *Water SA*, 46(3): 458-464. (No DOI available).

Fadaei-Kermani, E., Barani, G.A. 2014. Numerical simulation of flow over spillway based on the CFD method. *Scientia Iranica*, 21(1):91-97.

Fuladipanah, M., Azamathulla, H.M., Tota-Maharaj, K., Mandala, V., Chadee, A. 2023. Precise forecasting of scour depth downstream of flip bucket spillway through data-driven models. *Results in Engineering*, 20, p.101604. DOI: 10.1016/j.rineng.2023.101604

Karimaei Tabarestani, M. 2020. Study on stability and sensitivity analysis of protective riprap layer placed around bridge pier by using reliability analysis theory. *Journal of Hydraulics*, 14(4):51-68. DOI: 10.30482/jhyd.2020.105498.

Karimaei Tabarestani, M. 2021. Stability analysis of riprap layer at downstream of stilling basin based on reliability analysis. *Iranian Journal of Soil and Water Research*, 52(4):1163-1177. DOI: 10.22059/ijswr.2021.313692.668801

Lauchlan, C.S., Melville, B.W. 2001. Riprap protection at bridge piers. *Journal of Hydraulic Engineering*, 127(5):412-418. DOI: 10.1061/(ASCE)0733-9429.

Masjedi, A., Taeidi, A. 2017. Investigating the effect of roughness on the stability of stone slabs around the cylindrical foundation of the bridge in the river arch. *Journal of Water Engineering*, 10(32):1-12. (In Persian).

Mirzaee, R., Mohammadi, M., Mousavi, S.F., Bagherzadeh, M., Hosseini, K. 2023. Application of soft computing techniques to estimate the scouring depth formed by crossing jets. *Water Science & Technology*, 87(8):1853-1865. DOI: 10.2166/wst.2023.087

Parola, A.C., 1993. Stability of riprap at bridge piers. *Journal of Hydraulic Engineering*, 119(10):1080-1093. DOI: 10.1061/(ASCE)0733-9429.

Posey, C.J. 1974. Tests of scour protection for bridge piers. *Journal of the Hydraulics Division*, 100(12):1773-1783.

Rashki Ghaleh Non, M., Azhdary Moghaddam, M., Shafaei Bajestan, M., Azamathulla, H.M. 2020. Control of bed scour downstream of ski-jump spillway by a combination of six-legged concrete elements and riprap. *Ain Shams Engineering Journal*, 11(4):1047-1059. DOI: 10.1016/j.asej.2020.02.005

Salmati, S., Masoudian, M. 2025. Analysis of hydraulic performance of hinged sluice gate in spillway and gate modes, New Approaches in Water and Environmental Engineering, pp. 40–53. doi: 10.22034/nawee. 484734.1111

Worman, A. 1989. Riprap protection without filter layers. *Journal of Hydraulic Engineering*, 115(12):1615-1630. DOI: 10.1061/(ASCE)0733-9429(1989)115:12(1615)

Xiaolong, C., Ran, L., Jingjie, F., Zhu, D.Z., Kefeng, L. 2024. TDG generation in a ski-jump spillway with a fully or partial-flip bucket. *Journal of Environmental Management*, 353, p.120123. DOI: 10.1016/j.jenvman.2024.120123

Yoon, T.H., Yoon, S.B., Yoon, K.S. 1995. Design of riprap for scour protection around bridge piers. In: *26th IAHR Congress, UK*, 1:105-110.